Supporting Information

Field-Induced Slow Magnetic Relaxation in Mixed Valence Di- and Tri-nuclear Co^{II}-Co^{III} Complexes

Aparup Paul,[a] Marta Viciano-Chumillas,[b] Horst Puschmann,[c] Joan Cano,*[,b] Subal Chandra Manna,*[,a]

[a]*Department of Chemistry, Vidyasagar University, Midnapore 721102, West Bengal, India, E-mail: scmanna@mail.vidyasagar.ac.in, Fax: (91) (03222) 275329.*

[b]*Institut de Ciència Molecular (ICMol), Universitat de València, 46980 Paterna, València, Spain*

[c]*Department of Chemistry, University of Durham, South Road, Durham DH1 3LE, U.K.*

IR Spectral Studies

IR spectra of **1** and **2** are shown in Fig. S7 and Fig. S8, and a summary of the most important IR bands together with their tentative assignments are given in Table S5. The spectra of **1** and **2** exhibit strong bands at 3200–3600 cm^{-1} corresponding to the ν(O–H) stretching vibrations.[i] A strong and sharp band due to azomethine ν (C=N) appears at 1556 cm^{-1} and 1551 cm^{-1} for **1** and **2**, respectively. The strong bands at 1644 cm^{-1} (**1**) and 1640 cm^{-1} (**2**) are due to the anti-symmetric stretching mode of the carboxylate group, whereas the bands at 1414 cm^{-1} (**1**) and 1413 cm^{-1} (**2**) accord with the symmetric stretching modes of carboxylate. The bands at 2975 (**1**) and 2981 cm^{-1} (**2**) correspond to ν(C–H) (aromatic) stretching vibrations. ν(C–H) (aliphatic)

stretching vibration for **1** appears at 2943 cm^{-1}. $\nu(C_{ring}–O_{methoxy})$ stretching vibrations occur at 1298 cm^{-1} and 1302 cm^{-1} for complexes **1** and **2**, respectively. The bands at 1245 (**1**) and 1248 cm^{-1} (**2**) are ascribed to the $\nu(C–O_{phenolic})$ stretching vibrations.

[i] K. Nakamoto, Infrared Spectra of Inorganic and Coordination Compounds; John Wiley & Sons: New York, 1997

Table S1. H–bond parameters for complex **1**.

D–H···A	d(D–H)	d(H···A)	d(D···A)	<DHA	Symmetry A
O(10)–H(10E)···O(1)	0.79(3)	2.17(3)	2.952(3)	170(3)	1–x,1–y,–z
O(10)–H(10E)···O(2)	0.79(3)	2.40(3)	2.881(2)	120(3)	1–x,1–y,–z
O(10)–H(10F)···O(2)	0.77(3)	2.59(3)	2.881(2)	105(3)	1–x,1–y,–z
O(10)–-H(10F)···O(9)	0.77(3)	2.00(3)	2.746(2)	166(4)	1–x,1–y,–-z

Table S2. C–H···π interaction in complex **1**.

C–H	Cg(J)	H···Cg (Å)	X–H···Cg (º)	X···Cg (Å)
C(4)–H(4)	Cg(7)→C(15)-C(16)-C(17)-C(18)-C(19)-C(20)	2.89	163	3.812(3)
C(11A)–H(11B)	Cg(6)→C(1)-C(2)-C(3)-C(4)-C(5)-C(6)	2.98	148	3.852(5)
C(35A)–H(35A)	Cg(8)→C(23)-C(24)-C(25)-C(26)-C(27)-C(28)	2.76	161	3.708(6)

Table S3. C–H···π interaction in complex **2**.

C–H	Cg(J)	H···Cg (Å)	X–H···Cg (º)	X···Cg (Å)
C(18)–H(18)	Cg6→C(25)-C(26)-C(27)-C(28)-C(29)C(210)	2.82	131	3.519(5)
C(211)–H(21A)	Cg6→C(25)-C(26)-C(27)-C(28)-C(29)C(210)	2.52	143	3.356(5)

Table S4. H–bond parameters for complex **2**.

D–H···A	d(D–H)	d(H···A)	d(D···A)	<DHA	Symmetry A
O(2W)–H(2WA)···O(13)	0.90	1.77	2.654(5)	167	3/2–x,1+y,1–z
O(2W)–H(2WB)···O(3W)	0.79	2.14	2.874(4)	155	
O(3W)–H(3WA)···O(11)	0.85	1.89	2.731(5)	169	x,1+y,z
O(1W)–H(1WB)···O(3W)	0.83	1.97	2.776(5)	164	
O(1W)–H(1WA)···O(21)	0.82	2.08	2.855(4)	159	

Table S5. Experimental IR bands (cm^{-1}) of complexes **1** and **2**.

	1	**2**
ν(O–H) and ν(NH_2)stretching	3200–3600(br, vs)	3200–3600(br, vs)
ν(C–H) stretching (aromatic rings)	2975(s)	2981(s)
ν(C–H) stretching (aliphatic C–H)	2943(vw)	–
ν(C=N)	1556(vs)	1551(vs)
ν_{as}(C=O)	1644(s)	1640(s)
ν_{s}(C=O)	1414(vs)	1413(vs)
ν(ArC=C)	1466(s)	1468(s)
ν(C_{ring}–$O_{methoxy}$)	1298(vs)	1302(s)
ν_{s}(C–$O_{phenolic}$)	1245(w)	1248(s)
ν(C–N)$_{aliphatic}$	1078(vw)	1078(s)
ρ_{r}(H_2O)	880(vw),815(vw)	860(vw),814(vw)
ρ_{w}(H_2O)	768(vw)	779(vw)

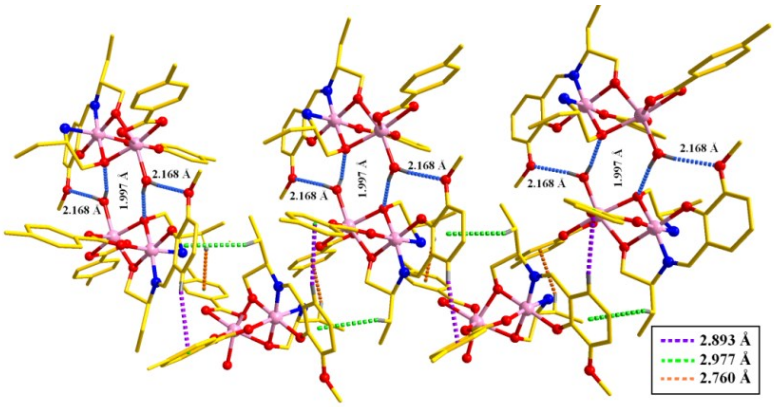

Fig.S1. 2D supramolecular structure of complex **1** through H–bonding and C–H···π interactions, disordered atoms are omitted for clarity.

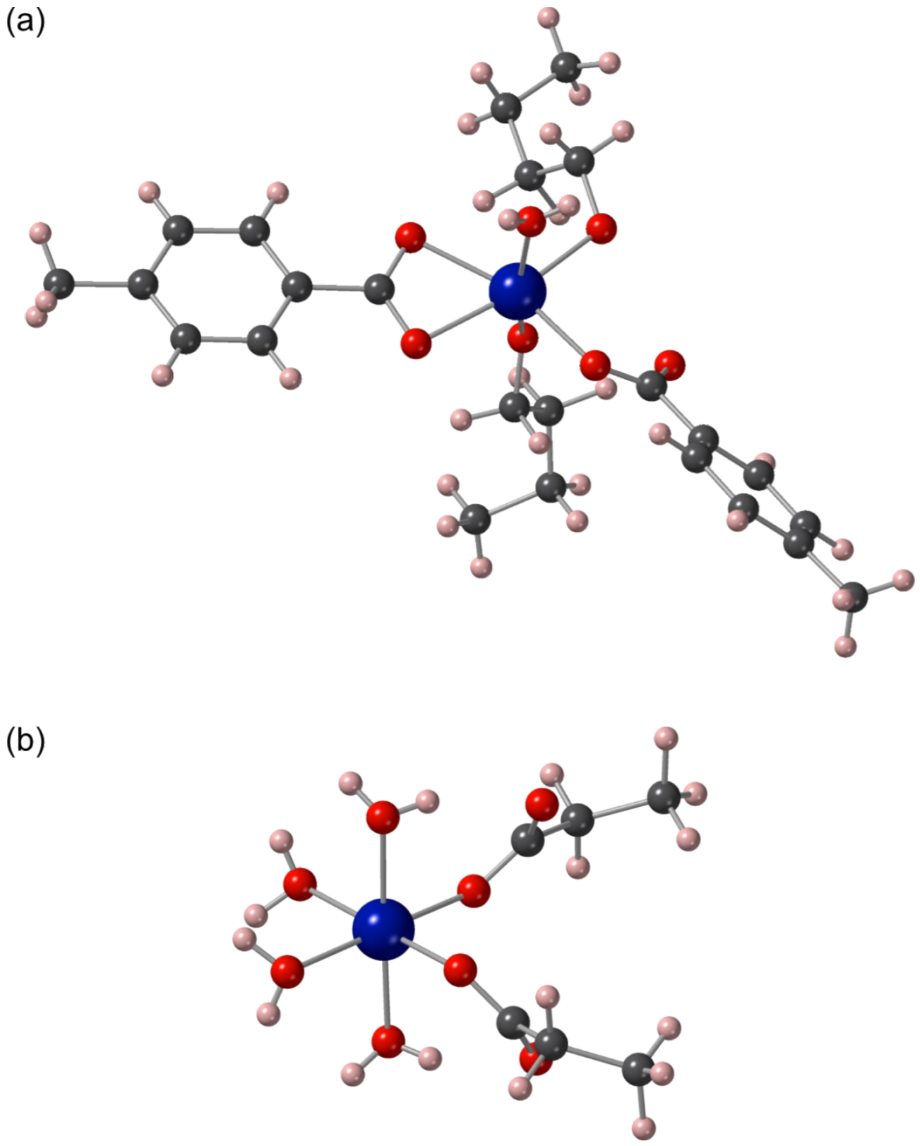

Fig.S2. Simplified mononuclear models built from experimental geometries of **1** (a) and **2** (b).

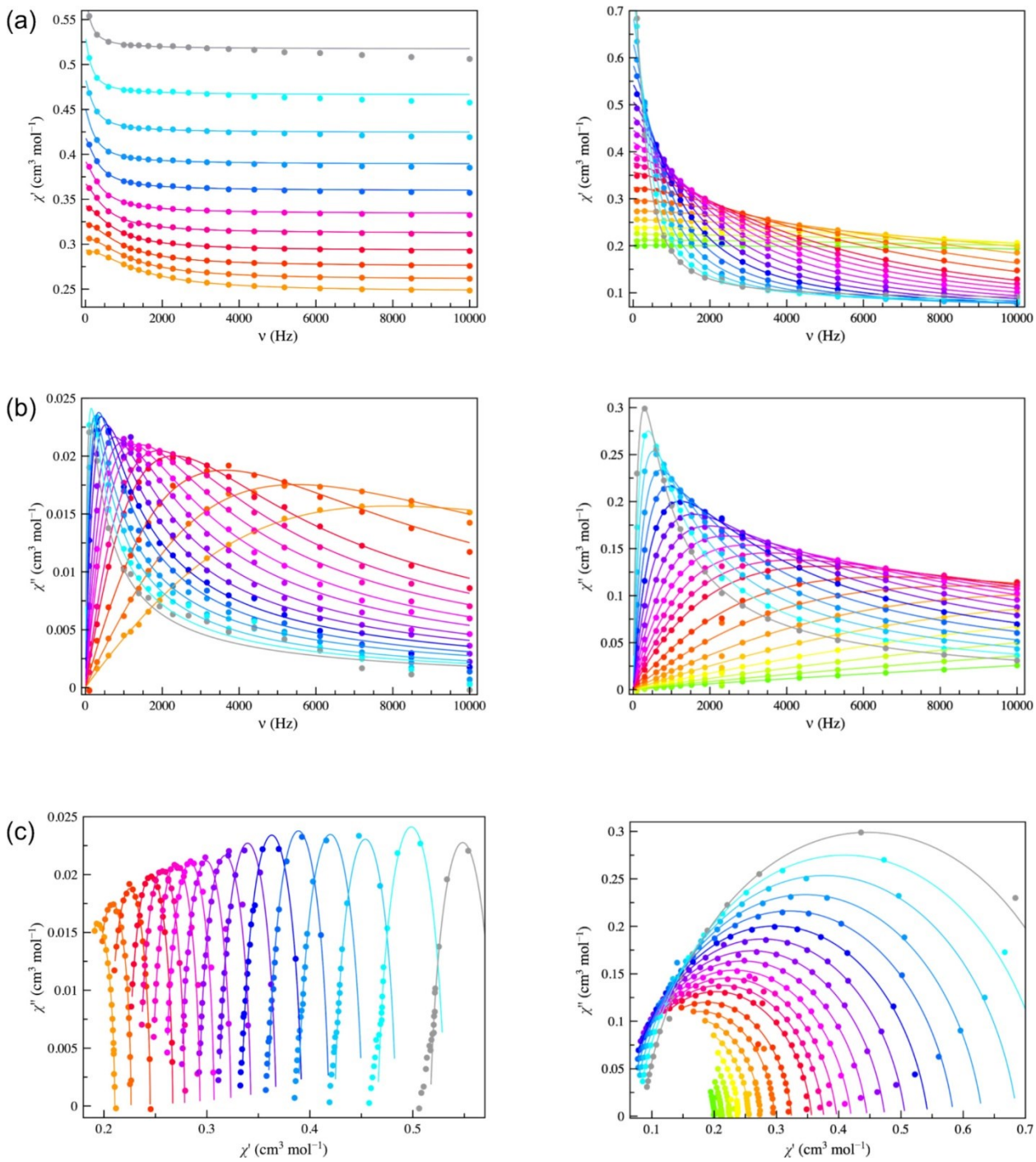

Fig.S3. Frequency dependences of χ_M' (a) and χ_M'' (b) and Argand plots (c) for **1** (left) and **2** (right) in a dc-applied static field of 1.0 kG with ± 5.0 G oscillating field in the temperature range of 2.0–6.5 (**1**) and 2.0–8.5 K (**2**) from grey to warmer colours in steps of 0.25 K below 5.0 K for **1** and 5.5 K for **2** and 0.50 K above these temperatures. The solid lines are the best-fit curves simulated using the values of χ_S, χ_T, τ and α shown in Figures 4 and S6.

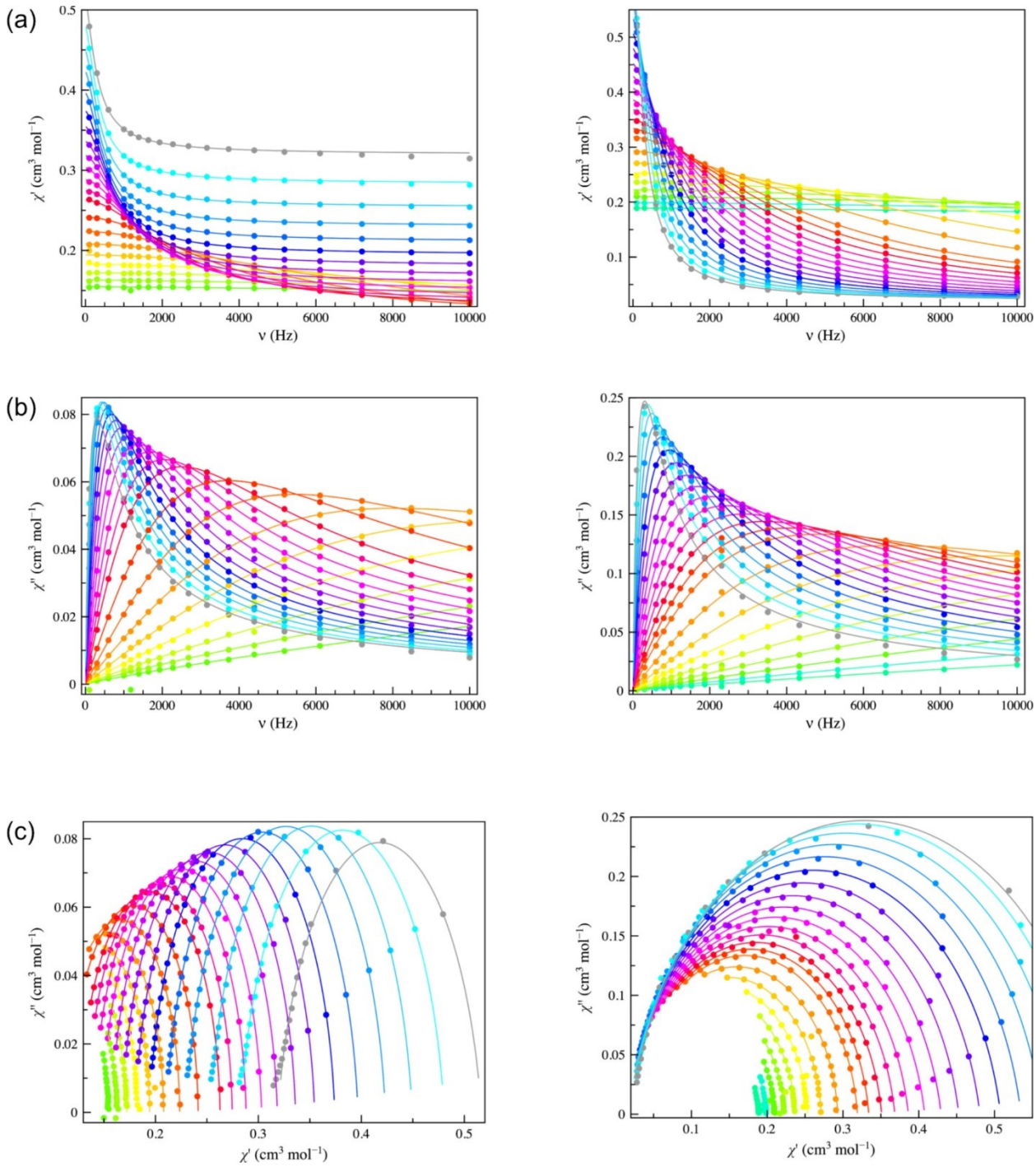

Fig.S4. Frequency dependences of χ_M' (a) and χ_M'' (b) and Argand plots (c) for **1** (left) and **2** (right) in a dc-applied static field of 2.5 kG with ± 5.0 G oscillating field in the temperature range of 2.0–9.0 (**1**) and 2.0–9.5 K (**2**) from grey to warmer colours in steps of 0.25 K below 5.0 K for **1** and 5.5 K for **2** and 0.50 K above these temperatures. The solid lines are the best-fit curves simulated using the values of χ_S, χ_T, τ and α shown in Figures 4 and S6.

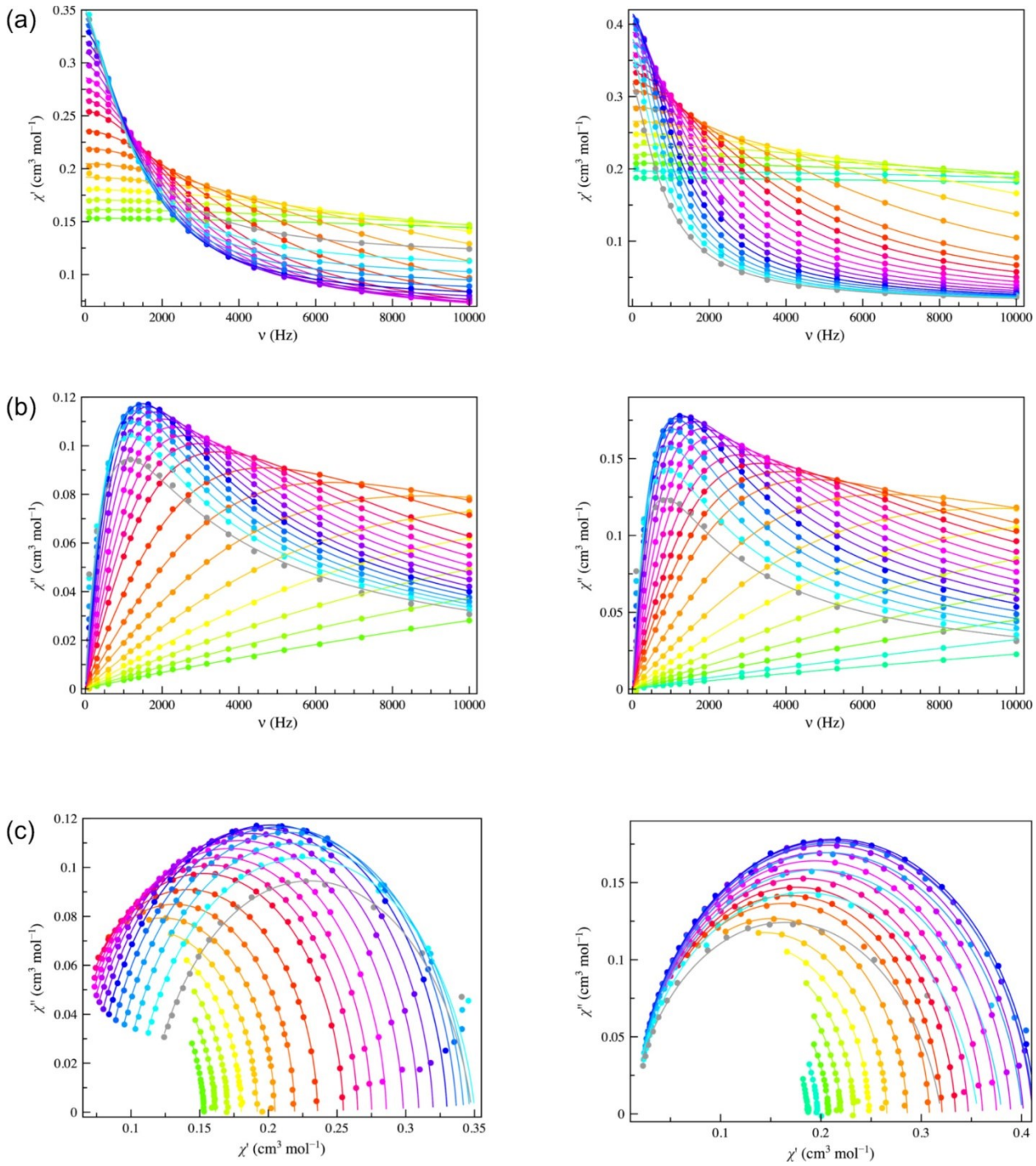

Fig.S5. Frequency dependences of χ_M' (a) and χ_M'' (b) and Argand plots (c) for **1** (left) and **2** (right) in a dc-applied static field of 5.0 kG with ± 5.0 G oscillating field in the temperature range of 2.0–8.5 (**1**) and 2.0–9.5 K (**2**) from grey to warmer colours in steps of 0.25 K below 5.0 K for **1** and 5.5 K for **2** and 0.50 K above these temperatures. The solid lines are the best-fit curves simulated using the values of χ_S, χ_T, τ and α shown in Figures 4 and S6.

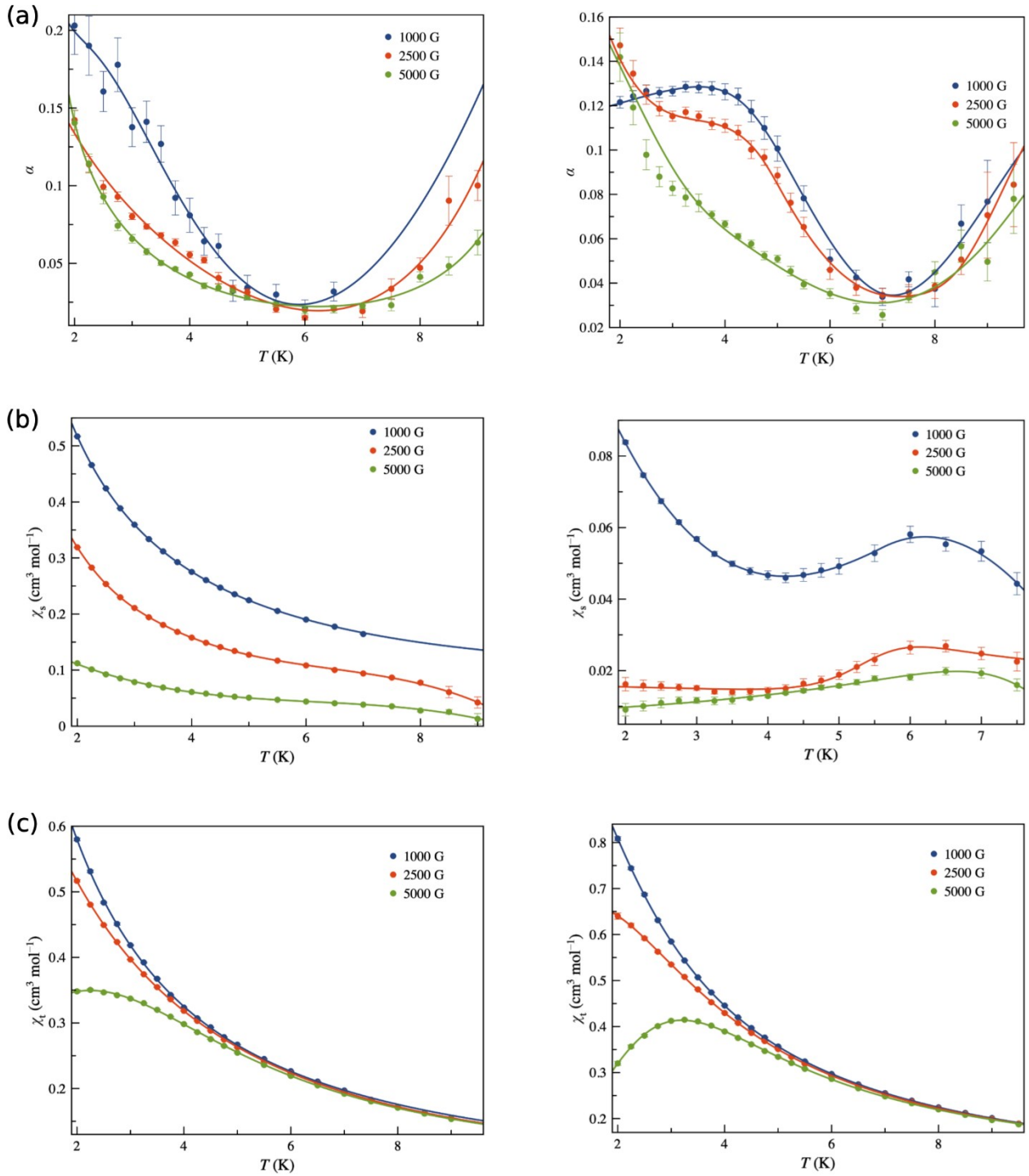

Fig.S6. Temperature dependence of α (a), χ_S (b), and χ_T (c) of **1** (left) and **2** (right) under applied dc magnetic field of 1.0, 2.5 and 5.0 kG. The solid lines are eye-guides. Standard deviations appear as vertical error bars.

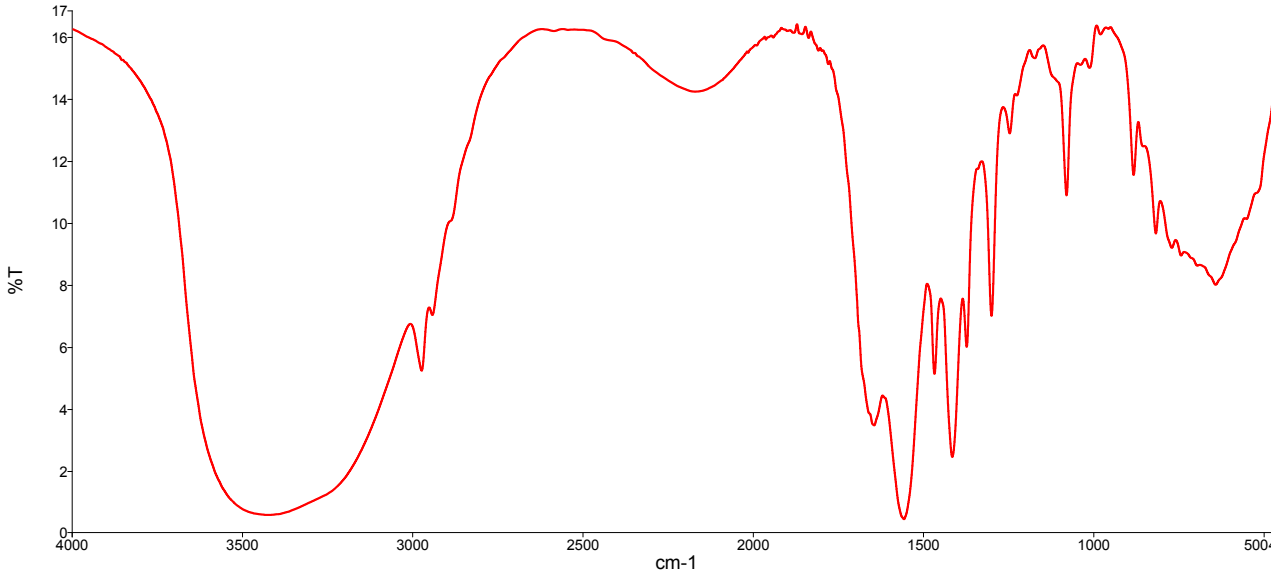

Fig.S7. IR spectrum of **1**.

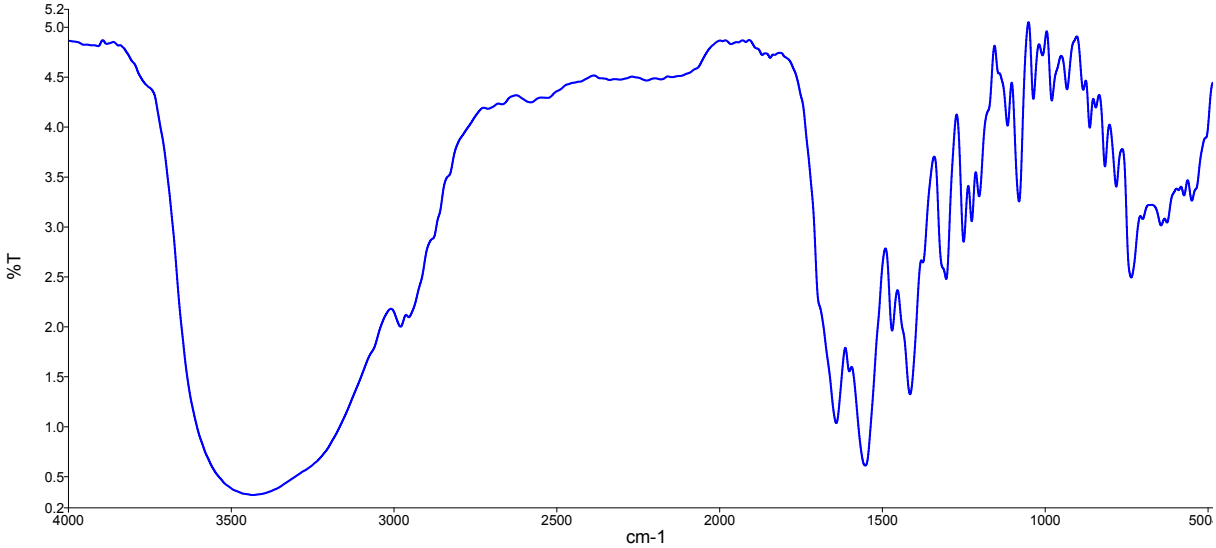

Fig.S8. IR spectrum of **2**.